Tungsten (2024) 6:196–211
https://doi.org/10.1007/s42864-022-00181-2

Tungsten
www.springer.com/42864

REVIEW PAPER

Recent development of three-dimension printed graphene oxide and MXene-based energy storage devices

Liang-Hao Yu[1,2] · Xin Tao[1] · Shang-Ru Feng[1] · Jin-Tao Liu[2] · Lin-Lin Zhang[1] · Guang-Zhen Zhao[1] · Guang Zhu[1]

Received: 24 June 2022 / Revised: 26 August 2022 / Accepted: 29 August 2022 / Published online: 10 October 2022

Abstract

The research for three-dimension (3D) printing carbon and carbide energy storage devices has attracted widespread exploration interests. Being designable in structure and materials, graphene oxide (GO) and MXene accompanied with a direct ink writing exhibit a promising prospect for constructing high areal and volume energy density devices. This review not only summarizes the recent advances in 3D printing energy storage devices including printing methods, ink rheological properties, and different energy storage systems, but also discusses the printing methods related to energy storage. In addition, the binder or additive free of two-dimensional carbide materials is quite important for the present electrochemical energy storage devices, which also are presented.

Keywords 3D printing · Two-dimensional materials · Energy storage device · Ink rheological · MXene

1 Introduction

With ever-increasing environmental consciousness and the development of sustainable syntheses, the development of new renewable energy has become a research hotspot. Therefore, "carbon peaking" and "carbon neutrality" have become the core issues for our countries in the coming decades. The electric energy generated by various renewable energy sources (such as wind energy and solar energy) usually encounters various problems such as uneven distribution, disordered waveform, and instability, which make it difficult to use directly. Therefore, many researchers have focused on electrochemical energy storage devices in recent years [1–4]. Among the numerous electrochemical energy storage devices (EESDs), the rechargeable batteries (REBs) and supercapacitors (SCs) can efficiently comply conversion of electrical and chemical energies through the transformation of ion and electron in electrodes, which plays an essential role in the EESDs [5, 6]. REBs such as lithium-ion batteries (LIBs), and sodium-ion batteries (SIBs) have attracted wide attentions in both academia and industry because of their high energy density (high gravimetric and volumetric energy density), low self-discharge and low cost. LIBs are considered as the most suitable devices for wide applications in large-scale energy storage systems, new energy vehicles and portable electronics. In contrast, SCs have high power density, low toxicity and long cycle life that are suitable for operation safety in the energy storage fields of wireless communications, multifunctional entertainments, and personal healthcare [7–9].

Previous EESDs fabrication primarily depends on conventional process, due to their mature fabrication procedures such as electrode rolling, cutting, separator assembly, electrolyte filling, and finally packaging devices [10]. These complex processes severely hinder their integration and production efficiently. Especially, in the manufacturing process of portable electronic devices, it is necessary to manufacture higher areal capacity in a small space [11–13]. At the same time, the increase of the active materials in a certain area can be an effective manner to improve the areal capacitance. However, the thick electrodes usually have uneven pores and long ion transport paths, which lead to the degradation of EESDs power density and rate performance. Additionally,

✉ Liang-Hao Yu
lhyu@ahszu.edu.cn

✉ Guang Zhu
guangzhu@ahszu.edu.cn

[1] Key Laboratory of Spin Electron and Nanomaterials of Anhui Higher Education Institutes, Suzhou University, Suzhou 234000, China

[2] Key Laboratory of Leather of Zhejiang Province, College of Chemistry and Materials Engineering, Wenzhou University, Wenzhou 325035, China

the traditional preparation of the electrodes with limited pore structures would result in a low utilization of active materials, thus hindering the electrode performances to reach a gratifying level. To maximize surface area accessibility and accelerate ion transport efficiency among electrodes, exploring advanced manufactured technology remains a decisive task besides the innovation of electrode materials [14–17].

Three-dimension (3D)-structured electrodes can be designed with hierarchical porous structures, which provides fast ion transport channels and makes full use of the limited space to obtain high energy density [18]. However, there are still remain limitations in the modulation of the geometry and structure of the solid electrolyte, because the inadequate electrolyte penetration, a slow ion transport significantly jeopardy the charge storage capability [19]. In conclusion, the main direction that researchers focus is on how to package high-energy density device with structure controllable EESDs in a small space.

3D printing, also called additive manufacturing technology, is a structure-editable bottom-up fabrication method. It allows the use of computers to manufacture three-dimensional frameworks with a high degree and integration [5, 20–24]. Compared with traditional manufacturing technologies, 3D printing has shown its value in manufacturing small batches and personalized materials, such as aerospace manufacturing and solid molding of human bones like teeth, thumbs and knees. With the development of industrialization that requires mass production, 3D printing can take advantage of its molding to provide customized samples for new structural [25–27]. Among EESDs, 3D printing technology can dramatically improve the material utilization rate, typically from the shape, size and structure design of energy storage devices. In addition, 3D printing technology also has the advantages of low cost, rapid manufacturing, uniform the electrode frame pore size, and micro-scale precise regulation [28–31]. Therefore, 3D printing technology can not only satisfy the existing forming process of materials, but also meet the challenges of exploring new structures. 3D printing technologies that have been developed for EESD manufacturing include inkjet printing (IJP) [32–34], material extrusion [including direct ink writing (DIW) [35] and fused deposition modeling (FDM)] [36], vat photopolymerization [such as stereolithography (SLA)] [37] and powder bed fusion [including Selective Laser Sintering (SLS)] [38]. Among them, DIW, IJP, FDM, SLS and SLA have been used to fabricate small-area miniature EESDs with well-designed patterns, controllable electrode thickness, and compatibility, as shown in Fig. 1. Furthermore, two-dimensional carbon-based materials such as graphene, and carbide like MXene, as the main ink material has received extensive attention in 3D printing [39–41].

Over the past few years, several reviews focusing on 3D printing with EESDs have been conducted. They are

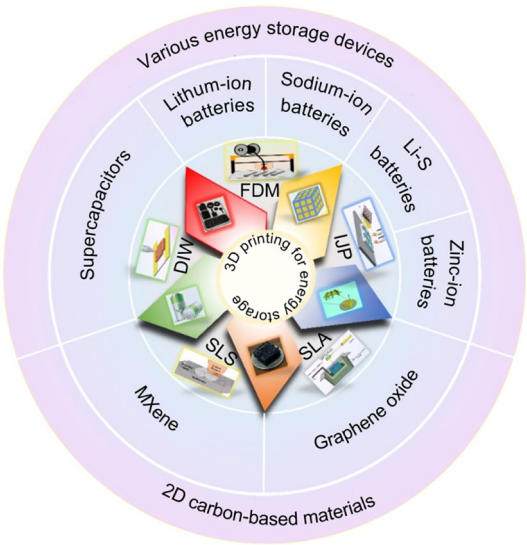

Fig. 1 A systematic map of "Ink material, 3D printing technology, and 3D printed structures" for EESDs

mainly concentrated on printing techniques, electrode patterns and application fields. However, summarizing carbon and carbide two-dimension (2D) materials as the bridges between substrate and active materials for 3D printing inks has acquired rare attentions in previous works.

In this work, we first summarize the different printing methods for 3D printing focused on their advantages and limitations. Then highlight DIW-based extrusion printing, also with the ink requires rheological properties [42]. Thereafter, the research progresses on novel 2D materials graphene oxide (GO) and MXene-based printable energy storage devices including, supercapacitors and rechargeable batteries are presented. Meanwhile, the several ink rheological properties adjusted work are also described, which aims at enhancing the device performance. Afterwards, binder- or additive-free inks, which are still in the initial stage of development, are introduced.

This review offers an outline on the development of printable strategies combined with the advantage of carbon and carbide among 2D materials, which may provide some ideas for future research directions.

2 3D printing techniques

2.1 Brief overview of 3D printing techniques

3D printing technology has been widely used in flexible energy storage and biomedical devices such as lithium-ion batteries and customization construction of bones [39, 43]. Comparing with traditional manufacturing technologies that impose mold requirements on materials, 3D printing

methods enable the bottom-up fabrications, which allows the use of computers to manufacturing three-dimensional frames containing complex spatial structures with a high degree of structural design and integration. Among the properties of 3D printing techniques, the most critical factors include ink material selection, patterning resolutions, pattern design versatility, printing speed, substrate of the print device and utilization rate. Several 3D printing methods that are used for energy storage device include FDM, selective laser melting (SLM), SLA, IJP and DIW. The schematic illustrations of these five techniques are shown in Fig. 1. In this review, 3D printing is equivalent to direct ink writing. This section presents the DIW printing principles, select and optimization of ink materials, pretreatment and post-treatment, parameter control and so on.

2.2 DIW method

DIW is an extrusion-based printing process, which was first designed to prepare ceramic materials then widely used in energy storage device. Compared with other 3D printing methods, the inkjet printing and extrusion printing offer the promising projects with the mass production of energy storage device [44–46]. As DIW, the ink can be extruded from the nozzle with compressed air. At the same time, the ink possesses a shear-thinning behavior to maintain its fluidity and high viscosity for the purpose of preventing material spreading on the substrate (Fig. 2a) [47]. DIW has many advantages such as easy operations, relatively lower cost, various materials selection such as polymer, ceramics and metal particles. However, it still faces the challenges of structural deformations after post-treatment [48, 49].

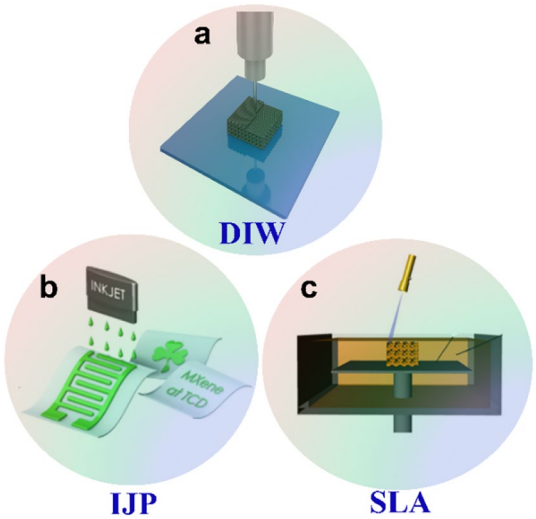

Fig. 2 Some 3D printing processes that are useful for energy storage preparation: **a** DIW. Reproduced with the permission from Ref. [47]. Copyright 2020 Nature. **b** IJP. Reproduced with the permission from Ref. [51]. Copyright 2019, WILEY-VCH. and **c** SLA. Reproduced with the permission from Ref. [24]. Copyright 2020 Springer

2.3 IJP method

IJP is a typical droplet-based deposition technique that can directly deposit materials through nozzles on to various substrates to create complex patterns with high resolution and tunable thickness corresponding to the number of droplets discharged [50]. As shown in Fig. 2b [51], the inkjet printing has the ability to print very complex basic frames as well as high ink utilization rate, which makes it one of the most eye-catching printing methods. However, due to the nozzle being easily blocked during the printing process, this technology has a high standard for ink and sacrifice the capability of preparing high mass loading electrodes [30, 52]. The ink requirement for IJP usually has specific requirements in surface tension, density and dynamic viscosity. The ink viscosity usually at the range of 5–50 centipoise (cP). However, DIW has high requirements for gel-based viscoelastic inks, requiring sufficiently high yield stress and storage modulus. The ink viscosity is usually over 1000 cP [53]. The deference between DIW and IJP technologies mentioned above are detailed in Table 1.

2.4 SLA method

SLA was invented in 1986 by Charles Hull, who also founded 3D Systems at the same time [54]. This technology focuses an ultraviolet (UV) laser into a bucket of photopolymer resin. The photosensitive resin will solidify when it encounters the UV laser (Fig. 2c) [24]. Thus, the pattern can be constructed under layer-by-layer method. It has a low production cost accompanied with the less preparation procedures. This printing process has been successfully applied to fabricate polymer substrates with different shapes and sizes. The SLA possesses an advantage of high resolution that will

Table 1 Comparisons of different technologies for DIW and IJP [5]

Technologies	Advantages	Disadvantages
Direct ink writing	Scalable, tunable thickness, material-saving, material diversity	Low-resolution electrode patterns
Inkjet printing	Precise control, scalable, efficient, low cost	Need of high-quality inks, relatively low-resolution electrode patterns

provide a delicate material structure which is important for special applications. However, the long duration of the manufacturing process and the limited scan rate of the laser also generate the obstacles to its development [55].

2.5 SLM method

Selective laser melting is an important part of 3D printing technology, which is proposed by the German Fraunhofer Research Institute in 1995 [56]. It is a rapid prototyping technology for metal, polymer and ceramic powders, which consists of a high-energy laser beam that fuses powder in a layer-by-layer process [57]. The processing technology and materials are the two key elements of SLM. The printing process of SLM consists of four parts. The first step is to apply a layer of extremely thin and uniform powder on the platform to build the model, and then use a laser technology to fully melt and fuse the powders according to the predesigned framework. The third step is to re-apply a new layer of powders on the platform, subsequently repeats the previous steps until the desired pattern is printed. Finally, removing the desired object from the printing platform. The printing process of SLM provides a novel method for printing chemical energy storage, which is cost-effective and convenient [58].

3 Rheological properties of two-dimensional sheet inks

3.1 Ink characterization: from Newtonian to shear-thinning solutions

The composition and the synergistic interaction between the components play a key part in the rheological properties of the inks, which affects printing characteristics of fluid inks. Generally speaking, when the ink is subjected to external force, the ink will deform to reduce the impact generated by this force. To describe the resistance of different components of the ink, a measurement of the viscosity (η) is introduced in this part. Among the rheological parameters, the viscosity is an indispensable element [59–62]. It is used to draw the frictional forces in the ink composition and calculated as the results of shear stress to shear rate. As shown in Fig. 3, the flow behavior of inks is described by the links of shear rate *vs.* its viscosity. In general, the behavior of various fluids can be divided into two parts: Newtonian behavior (liquid viscosity remains unchanged at different shear rates such as water, low molecular weight solvents.) and non-Newtonian behavior (both pseudoplastic and thixotropic properties describe as non-Newtonian behavior) [63]. To quantify the solution viscosity, a shear stress τ is applied to the ink contained at various geometry cells and the corresponding shear rate $\dot{\gamma}$ is measured. Moreover, the viscosity (η) is tested with the relation [64]:

$$\eta = \tau/(\dot{\gamma}). \tag{1}$$

Newtonian fluids, for example, the solutions like water behave as the τ varies linearly with the (γ) and the (η) is nearly constant as shown in Fig. 3a [63]. Bingham fluids, flow consistency index (k), flow behavior index n, a yield stress τ_0 and the shear stress is written as

$$\tau = \tau_0 + k\dot{\gamma}^n. \tag{2}$$

Moreover, the power law (PL) mode is set as Eq. (3), which results in Eq. (4)

$$\tau = k\dot{\gamma}^n = \eta(\dot{\gamma})\dot{\gamma}, \tag{3}$$

$$\eta(\dot{\gamma}) = k\dot{\gamma}^{n-1}. \tag{4}$$

Meanwhile, when $n < 1$, the ink exhibits a shear-thinning non-Newtonian fluid behavior (Fig. 3c). On the other hand, when $n > 1$, the ink exhibits a shear-thickening, which is harmful to printing process (Fig. 3b).

Figure 3e displays shear stress τ vs. shear rate $\dot{\gamma}$ and the viscosity acted as Eq. (5) for inks at different concentrations.

$$\eta = \frac{\tau}{\dot{\gamma}}. \tag{5}$$

At low poly(3,4-ethylene dioxythiophene):poly(styrenesulfonate) (PEDOT:PSTFSI) concentration, the solutions like water behave as Newtonian fluids as the τ varies linearly with the $\dot{\gamma}$ and the η is nearly constant as shown in Fig. 3a. Moreover, as the concentration increases (above 0.38%), the viscosity is varying with different $\dot{\gamma}$. It can be modeled using the power law (PL) model

$$\tau = k\dot{\gamma}^n. \tag{6}$$

In which, the higher shear rates correspond to a fluid with a PL fluid.

A liquid with this behavior is suitable for spray coating, screen printing, and extrusion printing. As for GO and MXene-based inks, the ink's viscosity and viscoelastic properties depend on the flakes' concentration in solvent. In Fig. 3f [65], both GO and its hydrogel ink exhibit the same shear-thinning behavior. Additionally, the rheological properties of different concentration MXenes show a clear viscosity decline with the increase of shear rates, which can satisfy an extrusion ink flow continuously (Fig. 3g) [59]. Furthermore, accompanied with the magnitude of viscoelastic moduli, the ratio of elastic modulus (G') to viscous modulus (G'') (G'/G'') plays another important role to determine the rheological properties of dispersion. For instance,

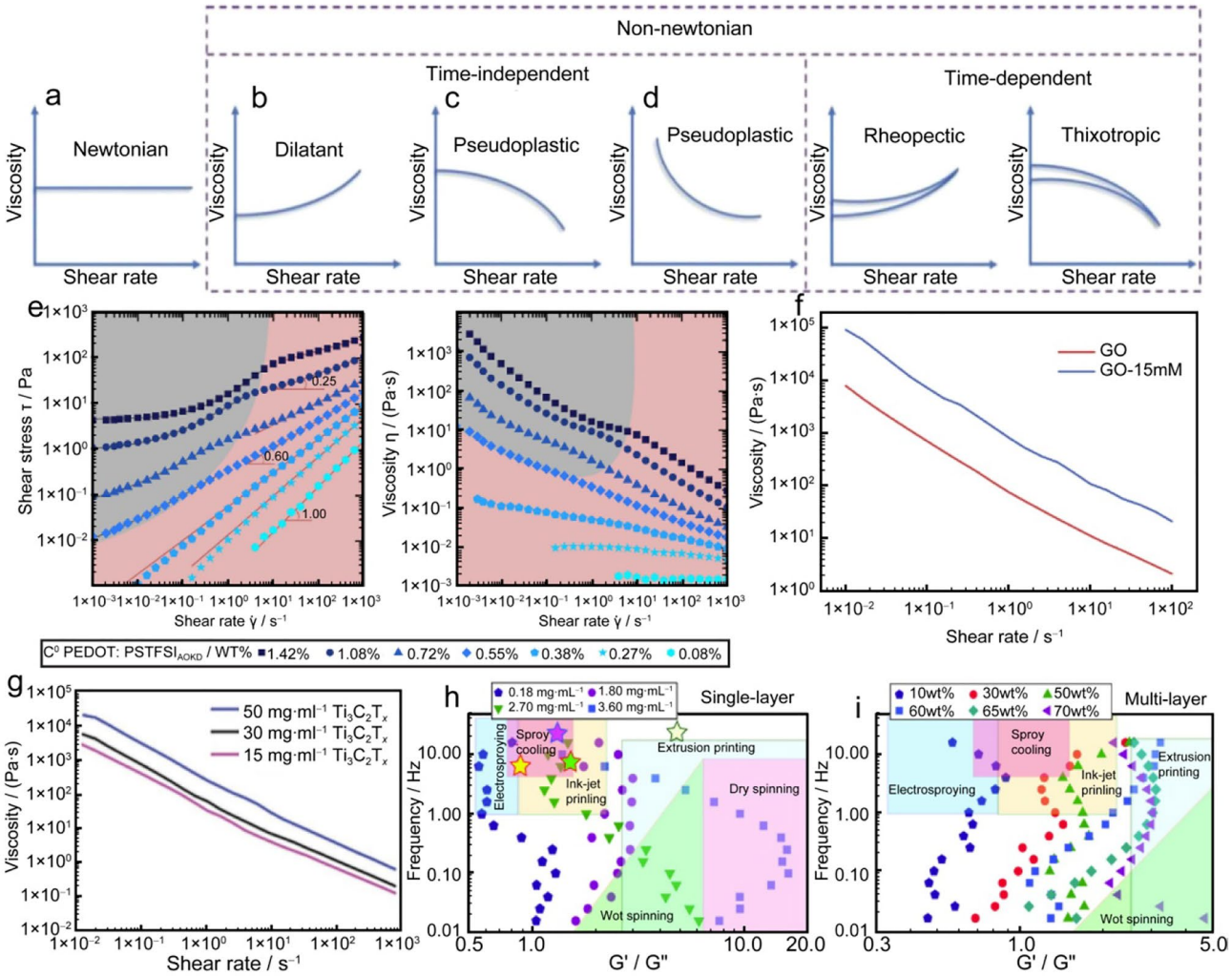

Fig. 3 **a**–**d** Overview of different shear profiles for various fluids. Reproduced with the permission from Ref. [63]. Copyright 2020 WILEY-VCH. **e** Rheological behavior of PEDOT:PSTFSI inks measured with a shear rheometer (cone plate geometry, 50 mm diameter and 1° angle). Reproduced with the permission from Ref. [64]. Copyright 2019 American Chemical Society. **f** Rheological behaviors of the GO pure solution and GO gel ink. Reproduced with the permission from Ref. [65]. Copyright 2018 WILEY-VCH V. **g** Rheological behaviors of the Ti3C2Tx solution with different concentration. Reproduced with the permission from Ref. [59]. Copyright 2020 American Chemical Society. **h**, **i** Frequency dependency of the ratio of the G' elastic modulus to G'' viscous modulus for single-layer Ti3C2Tx MXene flakes dispersed in water. Reproduced with the permission from Ref. [66]. Copyright 2018 American Chemical Society

the spray coating often requires a high viscous modulus ($G'/G'' < 1$) to maintain the ink continuous flow. On the contrary, extrusion printing requires elastic modulus with plastic-like properties over the mflow properties, which can help to preserve the shape of their printing patterns.

Motivated by this, Gogotsi et al.[66] found that single-layer $Ti_3C_2T_x$ seems to behave a high elastic modulus in a narrower mass percentage. Hence, it can be suitable for spray coating or inkjet printing process due to the high fluidity and versatile rheological properties of solutions (Fig. 3h). On the contrary, the range of G'/G'' ratios of the multilayer $Ti_3C_2T_x$ is much narrower than the single layer. Finally, the single and multilayer $Ti_3C_2T_x$ exhibit the unique but complementary rheological properties at different G'/G'' ratios (Fig. 3i). Interestingly, Yang et al. [67] found that 15 mg·mL^{-1} of single-layer MXene dispersions with a higher aspect ratio has a similar order of magnitude as 2.33 g·mL^{-1} multilayer MXene dispersions. Ultimately, the volatile solution accompanied with a low-frequency elastic component of single-layer GO or $Ti_3C_2T_x$ could help to construct the binder-free inks, which is quite important for electrochemical energy storage-related field.

4 3D printing energy storage device

Energy storage equipment is an indispensable part of mobile electronic equipment and new energy vehicles. Electrochemical energy storage devices can release energy through reversible physical or chemical reactions to keep electronic systems non-stop working [68, 69]. Particularly, supercapacitors and batteries with different energy storage mechanisms are two important components in our daily life, which will be illustrated in the following parts [13, 70–72]. Recently, the advantages of printing energy storage devices with high area loading and high energy density have become a research hotspot. Developing fully printed energy storage device necessitates formulating all these functional materials into printable inks. The property of the printed battery is largely dominated by the pattern size and resolution. Furthermore, they are extremely correlated with printing technologies, material properties of the inks (solid loading, viscosity, rheology behavior) [73]. Therefore, the development of easily printable functional materials accompanied with a high functionality is quite important [74, 75].

4.1 3D printing GO-based energy storage devices.

Graphene was first discovered in 2004, then GO has already achieved mass production [76]. To establish suitable printable ink, it is important to cultivate materials with high viscosity and shear-thinning behavior to facilitate 3D printing methods [77]. Lately, GO expresses a certain ability and unique viscosity properties as a liquid phase. Fortunately, ink viscosity can be adjusted by the graphene oxide concentration [78].

4.1.1 Supercapacitor

It is well known that SCs have the advantages of higher power density and fast charging/discharging ability [79]. Due to the different energy storage mechanisms, it can be classified into double layer and pseudocapacitive behaviors. For the former, an important feature is that no charge transfer occurs between the electrode and electrolyte interface, resulting in a lower energy density. Therefore, an enhanced ion transfer between electrolytes/electrodes can improve the energy density. Among various 3D printing technologies, such as FDM, SLM, DIW, and IJP have been widely used to design and fabricate the materials and structures related to SCs. 3D printing technology has the advantages of various adjustable properties related to material hardness, porosity, device shape and size, which enables to precisely control the electrode thickness and then regulate mass loading [80, 81].

Carbon and carbide materials possess ultra-high specific surface area, rich pore structure, good chemical stability, and mechanical strength that make them to be a suitable candidate for SCs, [40, 82, 83]. Among them, GO has a high surface area, excellent mechanical strength, thermal conductivity and adjustable viscosity, making it widely used in 3D-printed SCs devices. Previous work [84] suggests that specific polymers or colloidal templates introduced to ink compositions can promote the ink concentration with well-controlled viscoelastic responses. Therefore, chemical etching or additional thermal decomposition processes are necessary, which will increase the complexity of manufacturing and further slake the property of the target device. Thus, further efforts should be involved to achieve simplified ink design and structural control. Fan et al. [85] proposed a no sacrificial binder to develop hybrid inks and a uniform printing method by GO ink. The progressively releasing ammonium ions from urea in water can be electrostatically adsorbed by GO nanosheets. To control the rate of cross-linking, the pH was adjusted to nearly 3 by adding gluconic-δ-lactone, as shown in Fig. 4a. With the help of layer-by-layer construction method, diverse printing architectures like woodpile, honeycomb and more complicated patterns such as gearwheel could also be easily built (Fig. 4b). Furthermore, Gao and his co-workers [65] introduced Ca^{2+} as the cation into the GO solution. Then by the electrostatic adsorption between positive- and negative-charged materials (GO has oxygen-containing functional groups such as –COOH and –OH, therefore, Ca^{2+} ions can be used as cross-linkers), GO solution suddenly converts into the printable gel ink in a few minutes. In addition, to explore the gel transition caused by Ca^{2+} ions, they found that the G′ and τ were increased with the improve content of Ca^{2+} ions as shown in Fig. 4c. Especially, when the concentration of Ca^{2+}ions is over the limit of 15×10^{-3} mol·L^{-1}, the floccule of GO was observed. This unevenness caused by Ca^{2+} ions likely resulted from the clogging in nozzle and finally failed to printing. In this circumstance, GO (15×10^{-3} mol·L^{-1}) possesses the optimal rheological behaviors and its uniformity dispersion was chosen as the ink. We can observe in Fig. 4d, GO dispersion and GO–Ca^{2+} ink present the same non-Newtonian fluid behavior, in other words, the viscosity declined with the increasing of shear rates, which is necessary to guarantee the printable ink can flow smoothly. When the Ca^{2+}ions increased to 15×10^{-3} mol·L^{-1}, GO–Ca^{2+} ink exhibits the ten times higher apparent viscosity than that of pure GO solution. Accordingly, the *G′* also has a huge increase with the addition of Ca^{2+} ions. Subsequently, Ca^{2+} with a content of nearly 15×10^{-3} mol·L^{-1} was chosen as the target material. During following printing process, the ink was loaded into a movable injector, which is controlled by robot and extruded through a nozzle with pre-designed patterns. Then, freeze drying and HI reduction processes were introduced

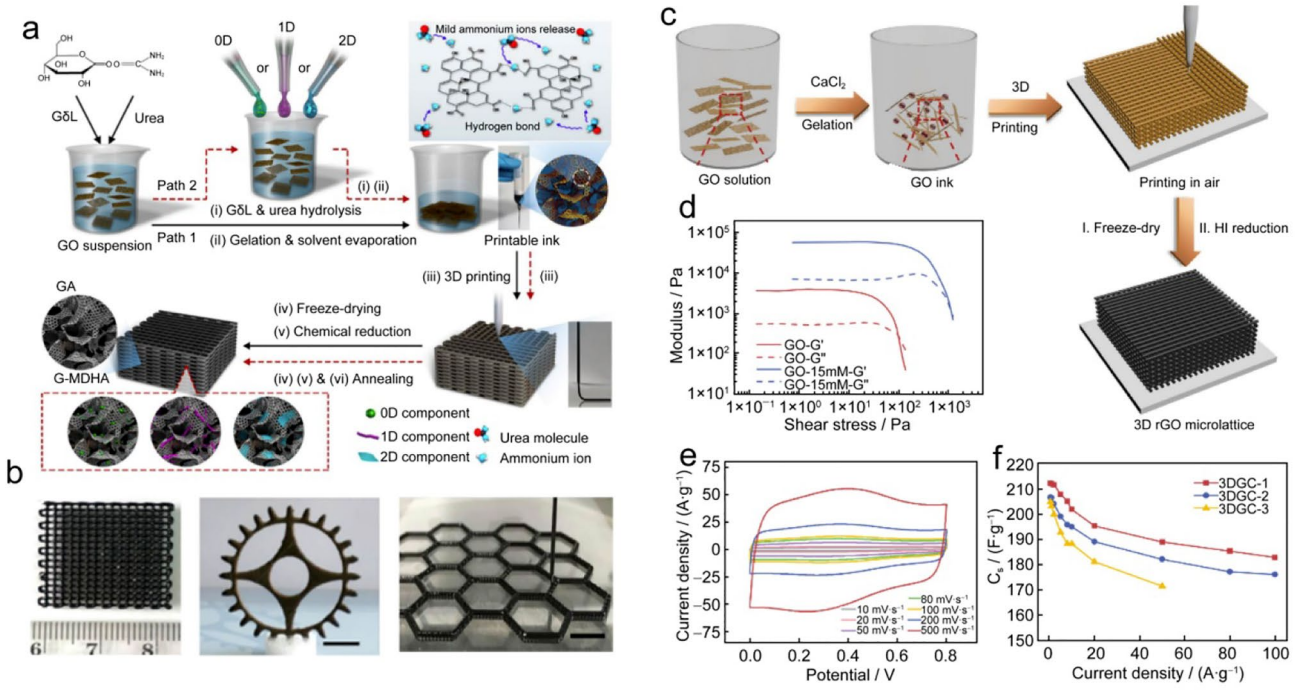

Fig. 4 **a** Proposed a no sacrificial binder to develop hybrid inks and uniform printing method by GO ink. **b** Diverse of the printed architecture. Reproduced with the permission from Ref.[85]. Copyright 2018 American Chemical Society. **c** Schematic illustration of 3D printing process typically with the trace amount of $CaCl_2$ is added into the GO solution to form GO ink. **d** The storage modulus and loss modulus of the GO pure solution and gel ink of shear stress. **e** CV curves for printed electrode at scan rates from 10 to 500 $mV{\cdot}s^{-1}$. **f** The comparison of different thickness electrodes at different current density from 0.5 to 100 $A{\cdot}g^{-1}$. Reproduced with the permission from Ref. [65]. Copyright 2018 WILEY-VCH

to remove water and convert into graphene; at the same time, we obtained a solid porous aerogel. The versatility of electrode architecture, which presents a porous structure, and graphene exhibits an excellent coherent conductivity, which is beneficial for supercapacitors. Figure 4e displays the cyclic voltammetry (CV) performance of supercapacitors with printed electrodes. The printed supercapacitor exhibits electrical double-layer capacitive (EDLC) behavior according to the quasi-rectangular-shaped CV curves. Fortunately, the electrodes show excellent electrochemical performances at different current density. At different current density (from 0.5 to 100 $A{\cdot}g^{-1}$), all the capacitance retention of print electrodes exceed 80%, and all the capacitors exhibit an outstanding rate performance, as shown in Fig. 4f. However, the energy density of supercapacitor cannot satisfy the practical application. According to the Eq. (7)

$$E = 1/2\,CV^2, \tag{7}$$

where the energy density (E) is relevant to the active material capacitance (C) and operation voltage (V) of device. On one hand, the capacitance value is mainly governed by the intrinsic properties of electrode materials. On the other hand, the voltage can be maximized by matching two electrodes with distinct voltage windows in an asymmetric cell configuration, further augmenting the energy density.

Li et al. [86] built a 3D graphene oxide structure by the direct ink writing method. The GO and hydroxypropyl methylcellulose acted as the basic skeleton material of the ink. After freezing dried and annealing in a noble gas, the aerogels of GO subsequently converted to porous graphene. In addition, the printed porous graphene aerogel lattice was elaborately designed as a structure for supporting pseudocapacitive MnO_2 nanosheets by electrodeposition, as shown in Fig. 5a. The deposition time from 0 to120 minutes, the 3D-printed GO achieved a super high mass loading of MnO_2 (~45 $mg{\cdot}cm^{-2}$). Importantly, both the volumetric and areal capacitance of the Graphene/MnO_2 electrodes increased nearly linearly accompanied with the increase of MnO_2 content at various current densities, as shown in Fig. 5b. It was attributed to the deposition of MnO_2 not only on the external surface, but also inside of the lattice. Owing to the electrodeposition of pseudocapacitive materials (MnO_2), the areal capacitance of Graphene/MnO_2 electrode is almost 25 times higher than pure graphene electrode that was tested at the same current densities (Fig. 5c). In this way, we can open up a new way to prepare the high mass loading and fabricate higher energy density supercapacitor.

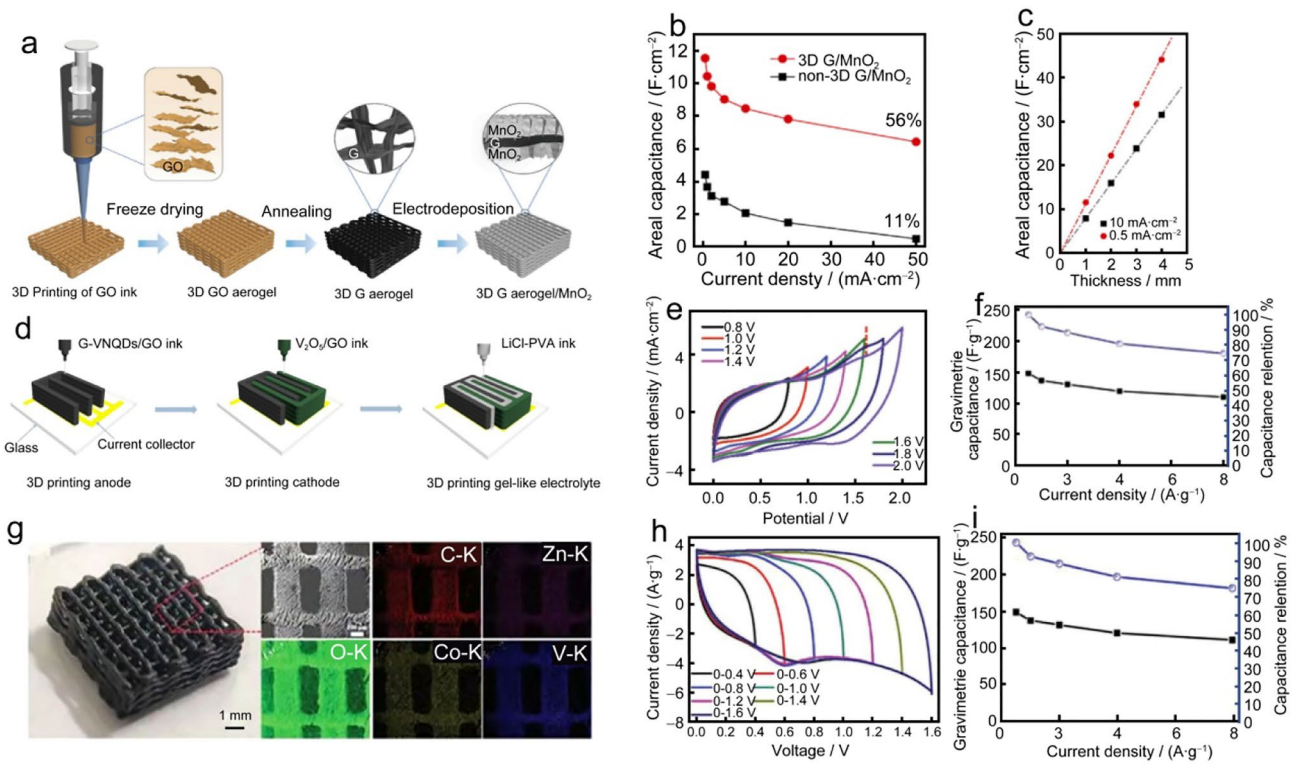

Fig. 5 **a** Schematic illustration of 3D construction graphene aerogel/MnO_2 Electrode. **b** Areal capacitances of 3D G/MnO_2 and non-3D printed G/MnO_2 electrodes obtained at different current densities of 0.5–50 mA·cm^{-2}. **c** Relationship between the thickness and areal capacitance. Reproduced with the permission from Ref. [86] Copyright 2019 Cell Press. **d** 3D printing process of electrode and electrolyte. **e**, **f** CV curves and different current densities of printed devices. Reproduced with the permission from Ref. [87]. Copyright 2018 WILEY-VCH. **g–i** 3D-printed asymmetric SCs device and the electrochemical performance. Reproduced with the permission from Ref. [46]. Copyright, 2019, WILEY-VCH

Furthermore, another method about asymmetric supercapacitor to increase energy density is provided by Yang [87] with interdigitated electrodes (V_2O_5/GO as cathode and G-VNQDs as anode). They are mixed with the highly concentrated GO gel forming the uniform solution, which will ensure the inks that possess a high viscosity and are suitable for DIW. Finally, the gel state electrolyte is also printed into the gap between the cathode and anode, schematic illustration of the 3D printing process is shown in Fig. 5d. The anode and cathode have different voltage ranges, they should maintain balance between high voltage output and stable redox potential. From a series of CV measurements determined the suitable voltage range is about 1.6 V (Fig. 5e). Due to the using of pseudocapacitive materials (G-VNQDs and V_2O_5) as well as asymmetric structure with high mass loading, which augment the areal energy and power densities (Fig. 5f). A higher areal energy density of 73.9 μW·h·cm^{-2} is acquired, which is superior to the most reported interdigitated Micro-Supercapacitors (MSCs), such as laser-scribed graphene, LIG–MnO_2, graphene quantum dots (GQDs)//MnO_2. Meanwhile, Yao et al. [46] used the same method to build a GO-based compound ink (ZnV_2O_6@$Co_3V_2O_8$–GO as positive and $Co_3V_2O_8$–GO as negative electrode). The 3D-printed pyre shape contains multiple orthogonal layers, then via scanning electron microscopy and energy dispersive spectroscopy demonstrate a uniform distribution of C, Zn, O, Co, and V in the electrode (Fig. 5g). Moreover, the asymmetric SCs device possesses the enlarged CV areas along with the increase of the voltages from 0.4 to 1.6 V in a two-electrode device (Fig. 5h). In addition, the printed patterns exhibit a superior rate capability of 78% at the range of 0.5–8 A·g^{-1}. We prospect that we can build asymmetric MSCs in a simple, low-cost and efficient manner by 3D printing (Fig. 5i).

4.1.2 Lithium-ion and beyond lithium-ion battery

LIBs are originated from lithium batteries. It is a new generation of electrochemical energy storage devices with outstanding advantages such as high voltage, high energy density output and remarkable cycle performance [88–91]. Therefore, in recent years, the research on LIBs has achieved extensive attentions. In 1982, Scrosati organized the first "Lithium Battery Conference" in Rome, attended by eighty

researchers, and this was the beginning of the lithium-ion story. Representative work about 3D printing batteries was from Lewis [91] that who fabricated interdigitated electrodes using 3D printer for a Li-ion micro-battery in 2013. They developed the concentrated inks with proper rheological behaviors to enable the 3D printing process. Their electrode inks consist of active materials (LFP for cathode and LTO for anode) and cellulose-based viscosity modifier. Owing to the lack of conductive agents, the cellulose-based electrode can supply electronic conductivity of 10^{-4}–10^{-6} S·cm^{-1}, which significantly restrict the electrochemical performance of printed battery. To improve the battery performance, GO is a good choice. It has superior electrical conductivity after thermal annealing or chemical reduction process. Heretofore, GO has been proven to be a candidate material in electrochemical storage device, especially in the LIBs [61, 62].

Hu et al. [92] proposed that $LiFePO_4$ (LFP) and $Li_4Ti_5O_{12}$ (LTO) inks were prepared separately and stored in cathode and anode syringes, individually. The schematic diagram of the 3D-printed LIBs is shown in Fig. 6a. Furthermore, they successfully fabricate the micro-interdigitated electrodes on glass substrate with barely 3 × 2 mm, as shown in Fig. 6b. Figure 6c shows the 3D-printed full packaged battery with LFP/rGO and LTO/rGO tested at 50 mA·g^{-1}, which exhibited a capacity of ≈100 mA·h·g^{-1}. This is a landmark work of 3D-printed GO-based LIBs, which opens new avenues for other battery systems. Yang and co-workers[93] fabricated orthogonal architectures Li–S batteries utilizing 3D printing process, where printable inks were prepared by S/DIB and S active materials into GO solution (4 mg·mL^{-1}). This work was the first time to propose Li–S batteries by 3D printing method and exhibited a higher reversible capacity of 812.8 mA·h·g^{-1}. The whole process is shown in Fig. 6d. The results show that graphene is useful for electrochemical energy storage owing to its superb highly chemical stability, electrical conductivity and large active site.

Recently, lithium and sodium-ion hybrid capacitors (LICs and SICs) have gained the growing research attentions, because they have both high energy and power characteristics by collaborating a battery anode (energy density) and a supercapacitor cathode (power density) [94, 95]. Compared with LICs, SICs have the advantages of natural abundance of resources and the low cost of sodium. As such, Sun and co-workers [94] developed 3D-printed SIC devices, which possess superior performances at power and energy output. Among the 3D printing process, the components and rheological properties of the ink, and the microstructure of pyre-shaped electrodes are the important branches. Figure 6e

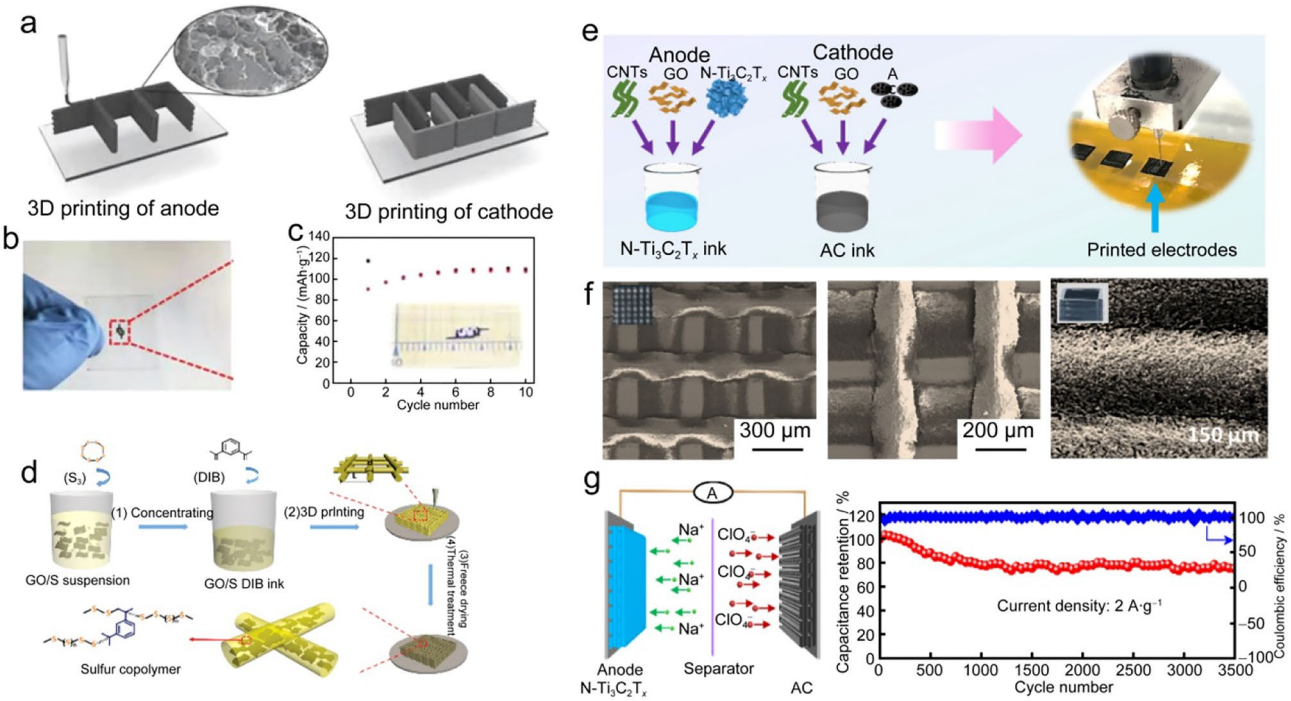

Fig. 6 **a** LTO/GO and LFP/GO ink used to fabricate the anode and cathode (in black) via layer-by-layer printing. **b**, **c** Digital images and electrochemical performance of a miniaturized version of the 3D-printed electrodes. Reproduced with the permission from Ref. [92]. Copyright 2016 WILEY-VCH. **d** Illustration of printed Li–S energy storage device. Reproduced with the permission from Ref. [93]. Copyright 2017 WILEY-VCH. **e** 3D printing process of the GO-based anode and cathode. **f** SEM images of the top view and side view of the 3D-printed N-$Ti_3C_2T_x$ electrode. **g** Schematic diagram of charging process of N-$Ti_3C_2T_x$ SIC and the cycle performance of the printed SIC at current 2 A·g^{-1}. Reproduced with the permission from Ref. [94]. Copyright 2020 American Chemical Society

displays the ink preparation procedure aimed at the formation of printed structure. Such the average and conductive inks contain active materials (N-MXene for the anode and AC for the cathode), CNTs as conductive agent, and GO as viscosity modifier in a certain weight proportion. After 3D printing and vacuum freeze drying, the electrodes can be solidified with ideal retention of the interior skeleton. From the side view and top view, SEM images of fabricated woodpile GO-based electrodes show continuously and tidily stacked piles as shown in Fig. 6f. It shows that the modified inks for printing are in high precision, which is indispensable to construct smooth erected electrodes with stable precision. Moreover, 3D-printed SIC full cells (woodpile-shaped electrode) were built up by GO-based N-$Ti_3C_2T_x$ and GO-based AC inks, as display in Fig. 6g. Based on charge balancing theory,

$$Q^+m^+ = Q^-m^-, \tag{8}$$

the appropriate mass ratio for anode and cathode can be calculated. The loading can be modified by the number of printed layers and the printed layers are proportional in relationship with the loading mass. The printed electrodes show a deviated triangle shape of the curves, which reveal a hybrid charge storage mechanism. Notice that the discharging and charging times are nearly the same at various current densities, meaning the high coulombic efficiency and excellent electronic conductivity. To demonstrate the stability of printed electrodes, the cycling performance of the devices was further tested. As exhibited in Fig. 6h, four layers show an excellent cyclic stability with a capacity retention of 75% above 3500 cycles at 2 A g^{-1}.

4.2 3D printing MXene-based energy storage devices

Recently, an emerging family of 2D transitional metal carbides called MXene with a universal formula of $M_{n+1}X_nT_x$ ($M_{n+1}X_nT_x$ [66, 96, 97], in which M represents an early transition metal such as Sc, Ti, V, Cr; X represents carbon and/or nitrogen and T represents the terminal functional groups n can be 1, 2, 3, 4), has displayed a great potential as electrode materials in building energy storage devices such as supercapacitors and batteries [98, 99]. Accordingly, MXene comes from the wet chemistry process with the typically surface terminations with –OH and –O. The introduction of surface –O functional groups was benefited to the uniform dispersion of suspensions into the solvent (such as ethanol, acetone, water, and ethylene glycol) and hence allows efficient formation of quite stable inks. In a low concentrations of MXene [100], the inks exhibit liquid-like behavior is suitable for spray coating and inkjet printing. Typically, the inks with highly concentrated MXene suspensions exhibit gel-like state with a high elastic modulus, making it more suitable for 3D printing [101]. Because of their viscosity, $Ti_3C_2T_x$ can be used as the binder and conductive additive for electrodes. Nicolosi et al. reported the using MXene nanosheets as a new type of binder as well as conductive agent to construct high volume change Si/MXene anodes without the need of any other additives [102].

Similar to the GO hydrogel and its gelation method, Yang et al. [103] reported a fast gelation of MXene in an aqueous solution with different metal ions such as Mg^{2+}, Co^{2+}, Ni^{2+}, Fe^{2+}, and Al^{3+}. It shows that the hydrogels can be constructed with the help of divalent and trivalent ions. The hydrogels possess G' and G'' among the whole frequency range, which is benefit for 3D printing.

At the same time, Kayali et al. [98] have demonstrated that controlling the size of MXene sheets can also improve the electrochemical performance. To have average size distribution, centrifugation is commonly used. Under this circumstances, the large size flakes with concentrated MXene solution by additive adoption or multiple centrifugation operations, which might lead to the agglomeration of MXene nanosheets.

4.2.1 MXene-based micro-supercapacitors (MSCs)

In recent years, flexible and stretchable electronics have boosted the rapid development in a wide variety of emerging applications such as implantable medical devices, wearable displays, and bioinspired electronic skin [104, 105]. The tortuous channels created by the flexible and stretchable electronics can be extensively used to develop high interdigital energy storage device, such as MSCs. As the important part of MSCs, electrode materials and device structures play key component in determining the device performance. Hence, the MXene with high conductivity and large charge storage capability, the interdigital structure with rich open edges, high mass loading of active materials, and free of conventional separator have attracted widespread attention [106].

For example, Barg et al. [67]. established an aqueous ink with the most reported MXene material $Ti_3C_2T_x$ by wet etching (HCl + LiF) procedure followed by a delamination protocol (without sonication steps). Subsequently, an ideal viscoelastic property with a shear-thinning behavior by extrusion-based printing was constructed with a freestanding 3D architecture, as shown in Fig. 7a. Freeze drying technology retains the external formation and internal integrity, the results show that the prepared $Ti_3C_2T_x$ inks' viscoelastic properties are suitable for 3D printing of freestanding architectures. Besides, the porosity can lead to the more effective active surfaces for the electrolyte and further improve rate performances. For the sake of extending potential of MXene inks, a 3D-printed interdigitated electrodes with tunable finger thickness can be as small as 100 µm (Fig. 7b, c).

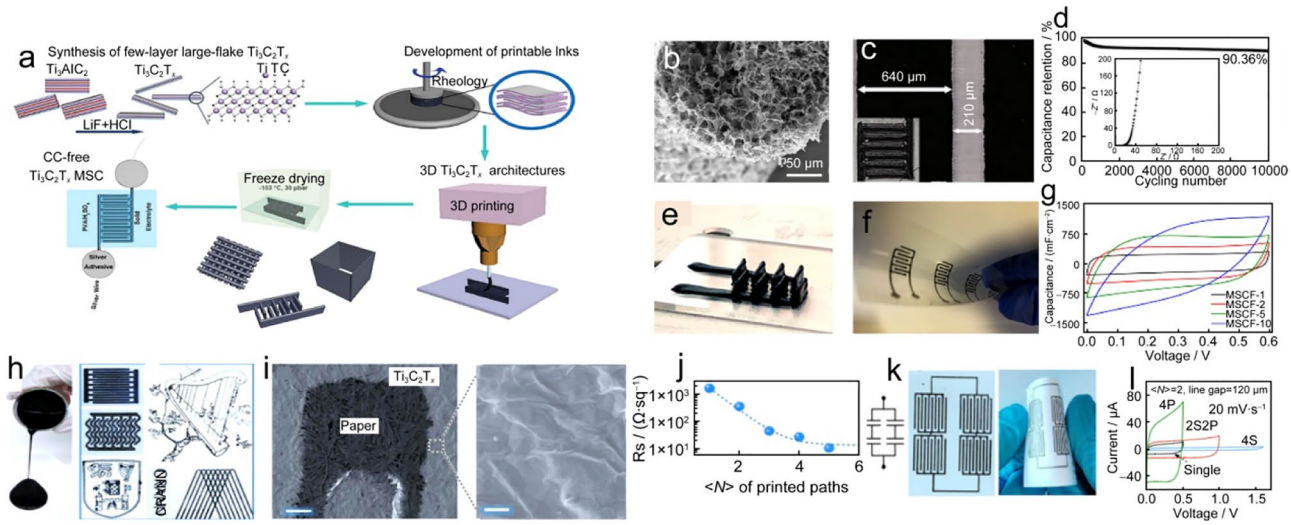

Fig. 7 Additive-free MXene inks. **a** Schematic representation of the manufacturing strategy developed for 3D printing of freestanding MXene architectures and MSC demonstrators. **b**, **c** SEM and optical photographs (inset) of freestanding $Ti_3C_2T_x$ microstructure and 3D-printed interdigitated structure. **d** Cycling stability test showing over 90% capacitance retention after 10,000 cycles at 1 $A{\cdot}g^{-1}$. Reproduced with the permission from Ref. [67], Copyright 2019 WILEY-VCH. **e**, **f** Printing tunable finger thickness on various substrate. **g** CV curves at 5 $mV{\cdot}s^{-1}$ for different mass loading. Reproduced with the permission from Ref. [98]. Copyright 2018 American Chemical Society. **h** Photo of MXene aqueous ink and printed patterns. **i** Low and high magnification SEM image of printed interconnected MXene MSC (Scale bar 200 μm, 500 nm, respectively). **j** The sheet resistance, Rs with number the printed paths. **k**, **l** Extrusion-printed tandem devices with great flexibility and typical CV curves of the as-printed tandem devices. Reproduced with the permission from Ref. [51]. Copyright 2019 Nature

Furthermore, to evaluate the electrochemical performance, the interdigitated symmetrical electrode architectures were tested with H_2SO_4/polyvinyl alcohol (PVA) gel electrolyte. Notably, the printed MSCs revealed extraordinary cycling performance with only 10% capacitance fade after 10,000 cycles at 1 A g^{-1} (Fig. 7d). Moreover, Beidaghi et al. [98] utilized high-concentrated $Ti_3C_2T_x$ inks without additives exhibits appropriate extrusion viscoelasticity and used to fabricate all solid state MSCs with various thickness on different substrates (Fig. 7e, f). The 3D printing devices with various mass loading represent excellent electrochemical performance at a 5 $mV{\cdot}s^{-1}$ scan rate, which areal capacitance reach to as high as 1035 $mF{\cdot}cm^{-2}$, as shown in Fig. 7g.

MXene-based materials are theoretically excellent materials for flexible MSCs; however, amalgamating nanomaterials with superb charge storage capability into low-price manufacturing process remains challenging. Direct ink writing like inkjet and extrusion printing of functional materials offers digital and additive patterning, increased material utilization, scalable and rapid production, and so on. Zhang et al. [51] fabricated MSCs through an extrusion printing method with additive-free and interdigitated devices on paper substrate. Due to the ideal fluidic properties, various fine patterns can be printed (Fig. 7h). For example, printing two paths gives MSCs behave line gap ~ 120 μm, width ~ 438 μm and spatial uniformity within ~ 5.6% (Fig. 7i). Particularly, exponentially decayed resistance from 2000 to 10 $\Omega{\cdot}sq^{-1}$ of the printed lines can be realized by increasing the printing numbers (Fig. 7j). It exhibits the possibilities of current collectors and conductive agents, due to the metallic conductivity. Moreover, depending on the hydrogen bonds between the interconnected layers cause a strong adhesion, which is enable to the mass production of all-MXene printed MSCs. In addition, to meet the energy or power requirements, the flexible and interactable MXene-based array MSCs can be fabricated in series and parallel (Fig. 7k). Then, the as-printed array devices are tested with CV curves at 20 $mV{\cdot}s^{-1}$, such as printing two in parallel and in series and four MSCs in parallel and in series (Fig. 7l). As printed MSCs display the excellent mechanical flexibility, which can be attributed to the mechanical strength of $Ti_3C_2T_x$ nanosheets and strong hydrogen bonds between the flakes.

4.2.2 Additive free of MXene-based EESDs

To the best of our knowledge, the fully printable fabrication of energy systems with binder-free (without polymer binder) ink is still challenging [107]. And the extrusion-based electrochemical energy storage device with higher energy density is still in its infancy [108]. The abundant functional surface terminations and superior mechanical characteristic permit MXene to form a hierarchically viscoelastic substrate [109]. Wu et al.[101] fabricated pure MXene ink on the

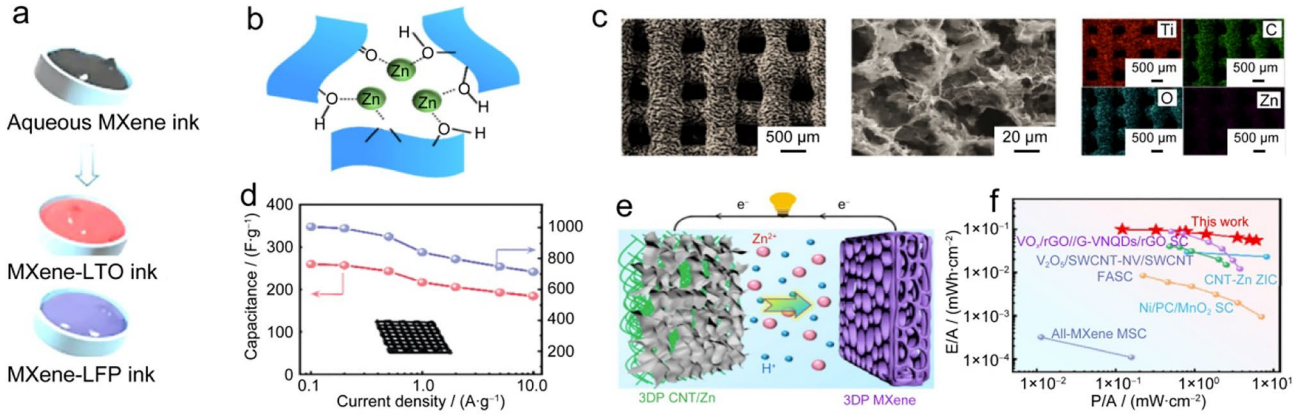

Fig. 8 **a** Schematic illustration of additive-free aqueous MXene-based LTO and LFP inks. Reproduced with the permission from Ref. [101]. Copyright 2021 WILEY-VCH. **b** Zn^{2+} gelation process targeting the preparation of MXene ink. **c** Top-view SEM images and corresponding EDS maps of the MXene. **d** Mass and area specific capacitance values at different current densities. **e**, **f** Schematic diagram and Ragone plots of the 3DP ZIC full cell. Reproduced with the permission from Ref. [111]. Copyright 2021 American Chemical Society

substrate as the current collector. Then, two different kinds inks such as MXene-based LFP and LTO were prepared, which were printed on the substrate, individually (Fig. 8a). This is a new attempt to take full advantages of the MXene (MXene acts as a highly capacitive electrode, conducting interconnect, current collector, and adhesive additive).

In addition to LIBs, Zn-ion hybrid capacitors (ZICs), which utilize capacitor-type cathode and a matched zinc battery type anode have high energy and power characteristics [110]. Sun's [111]group successfully demonstrated an 3D-printed MXene-based ZIC cathodes as shown in Fig. 8b, c. In this work, a trace amount of Zn^{2+} worked as cross-linkers to obtain a binder-free inks. The constitution of gel mostly suppresses the restacking of MXene flakes and promotes electrolyte penetration. The as-printed aqueous rechargeable ZICs possess the excellent rate capability of 184.4 $F{\cdot}g^{-1}$ at discharge current of 10 $A{\cdot}g^{-1}$ and reversible areal capacity of around 1006.4 $mF{\cdot}cm^{-2}$ at discharge current of 0.38 $mA{\cdot}cm^{-2}$, which are currently the highest value among 3D-printed capacitor devices. Moreover, the as-integrated ZIC device achieved a reversible areal power density of 5.9 $mW{\cdot}cm^{-2}$ (Fig. 8d–f).

5 Conclusion and outlook

Printable technology has promising potential for fabrication of power supply devices. Notably, 3D printing EESDs is a new and quickly developing technology that has a huge influence on next generation electronics. Herein, we first summarize the different printing methods for 3D printing focused on their advantages and limitations, and followed by highlighting the DIW-based extrusion printing and the ink required rheological properties. Thereafter, the research focus on novel 2D materials GO and MXene-based printable energy storage devices, including supercapacitors and rechargeable batteries are presented. The research progresses in device construction and performance enhancement due to the unique properties of GO and MXene two-dimensional nanosheets structures are highlighted. The attractive properties of printable ink component and design requirements to enhance ink rheological properties with excellent printability are further discussed. Of note, the ink with higher elastic modulus ($G'/G'' > 1$) can be suitable for 3D printing. Meanwhile, several ink rheological properties adjusted work are described, which aim at enhancing the device performance. Afterwards, binder- or additive-free inks, which are still in the initial stage of development, are introduced.

Recent achievements have provided the innovative routes in printing process, materials screening and architecture revolutions for printing various energy storage devices. However, there are still several challenges to be addressed before widespread utilization.

In the first place, the energy storage device by 3D printing technique is still in its infancy. We are simply fabricating the device layer by layer, thinking about the rheological properties of the ink (binder, conductive agent, and active materials), and constructing a very small samples to use. For practical application, the compatibility with other manufacturing processes is quite indispensable, which needs the high scalability. Therefore, modifying the device structure and choosing ink materials are essential. For instance, materials contain high aspect ratio fillers or nanosheets, which can be easy to agglomerate and cannot flow through small nozzles, which restrict the selection of materials and lower the printing accuracy. Particularly, for the small size electronics, one of the main factors to improve the energy storage capability is to achieve a high printing resolution.

Second, 3D printing has the capability of tailoring the thickness of electrodes to increase the volumetric capacitance and energy density compared to bulky electrodes at the same level. Unfortunately, the most electrodes at extremely high mass loadings will restrict the ion diffusion, which is lacking in competitiveness with traditional techniques like evaporation, electrochemical deposition and sputtering. Therefore, the dedicated research efforts should be focused on modifying printable ink with proper viscosity and porosity, to realize efficient conductive channels. Apart from these, the well-controlled interface on the substrate with flexible properties is another important factor.

Finally, it is still challenging to construct all the components such as electrodes, separator, and packaging via 3D printing. Furthermore, to meet the requirement of integrated with smart electronics is called "internet of things (IoT)", such as environmental or health monitoring and external or implantable electronics, it is particularly wished to achieve fully fabrication of energy storage by 3D printing. The intelligent design is versatile to robust and seamless with high ion conductivity as well as mechanical compliance, which satisfies the protective characteristic.

Acknowledgements This work was financially supported by the Natural Science Research Project in Universities of Anhui Province in China (No. K J2020A0727), the Key Discipline of Material Science and Engineering of Suzhou University (No.2017XJZDXK3), the Doctor of Suzhou University Scientific Research Foundation Project (No.2020BS014), the Graduate Research and Innovation Fund of Suzhou University (No.2021KYCX11), the platform of Suzhou University (No.2021XJPT16).

Declarations

Conflict of interest The authors declare no interest conflict.

References

1. Liu XH, Jervis R, Maher RC, Villar-Garcia IJ, Naylor-Marlow M, Shearing PR, Ouyang M, Cohen L, Brandon NP, Wu B. 3D-printed structural pseudocapacitors. Adv Mater Technol. 2016;1:1600167.
2. Wu FF, Li RY, Huang LC, Miao H, Li X. Theme evolution analysis of electrochemical energy storage research based on CitNetExplorer. Scientometrics. 2016;110:113.
3. Guo RQ, Zhang LX, Lu Y, Zhang XL, Yang DJ. Research progress of nanocellulose for electrochemical energy storage: a review. J Energy Chem. 2020;51:342.
4. Shinde PA, Jun SC. Review on recent progress in the development of tungsten oxide based electrodes for electrochemical energy storage. Chemsuschem. 2020;13:11.
5. Egorov V, Gulzar U, Zhang Y, Breen S, Odwyer C. Evolution of 3D printing methods and materials for electrochemical energy storage. Adv Mater. 2020. https://doi.org/10.1002/adma.202000556.
6. Escobar B, Martínez-Casillas DC, Pérez-Salcedo KY, Rosas D, Morales L, Liao SJ, Huang LL, Shi X. Research progress on biomass-derived carbon electrode materials for electrochemical energy storage and conversion technologies. Int J Hydrogen Energy. 2021;46:26053.
7. Brown E, Yan P, Tekik H, Elangovan A, Wang J, Lin D, Li J. 3D printing of hybrid MoS2-graphene aerogels as highly porous electrode materials for sodium ion battery anodes. Mater Des. 2019;170: 107689.
8. Delmas C. Sodium and sodium-ion batteries: 50 years of research. Adv Energy Mater. 2018;8:1703137.
9. Liu J, Wang BQ, Sun Q, Li RY, Sham T-K, Sun X. Atomic layer deposition of hierarchical CNTs@$FePO_4$ architecture as a 3D electrode for lithium-ion and sodium-ion batteries. Adv Mater Interfaces. 2016;3:1600468.
10. Gulzar U, Glynn C, Odwyer C. Additive manufacturing for energy storage Methods, designs and material selection for customizable 3D printed batteries and supercapacitors. Curr Opin Electrochem. 2020;20:46.
11. Yuan SJ, Fan W, Wang D, Zhang LS, Miao YE, Lai FL, Liu TX. 3D printed carbon aerogel microlattices for customizable supercapacitors with high areal capacitance. J Mater Chem A. 2021;9:423.
12. Pham MH, Khazaeli A, Godbille-Cardona G, Truica-Marasescu F, Peppley B, Barz DPJ. Printing of graphene supercapacitors with enhanced capacitances induced by a leavening agent. J Energy Storage. 2020;28:101210.
13. Wang ZS, Zhang QE, Long SC, Luo YX, Yu PK, Tan ZB, Bai J, Qu BH, Yang Y, Shi J, Zhou H, Xiao ZY, Hong WJ, Bai H. Three-dimensional printing of polyaniline/reduced graphene oxide composite for high-performance planar supercapacitor. ACS Appl Mater Interfaces. 2018;10:10437.
14. Li GJ, Mo XY, Law W-C, Chan KC. 3D printed graphene/nickel electrodes for high areal capacitance electrochemical storage. J Mate Chem A. 2019;7:4055.
15. Lee HM, Muralee Gopi CVV, Rana PJS, Vinodh R, Kim S, Padma R, Kim H-J. Hierarchical nanostructured $MnCo_2O_4$–$NiCo_2O_4$ composites as innovative electrodes for supercapacitor applications. New J Chem. 2018;42:17190.
16. Liu SM, Cai YJ, Zhao X, Liang YR, Zheng MT, Hu H, Dong HW, Jiang SP, Liu YL, Xiao Y. Sulfur-doped nanoporous carbon spheres with ultrahigh specific surface area and high electrochemical activity for supercapacitor. J Power Sources. 2017;360:373.
17. Saleh MS, Li J, Park J, Panat R. 3D printed hierarchically-porous microlattice electrode materials for exceptionally high specific capacity and areal capacity lithium ion batteries. Addit Manuf. 2018;23:70.
18. Cheng M, Jiang YZ, Yao WT, Yuan YF, Deivanayagam R, Foroozan T, Huang ZN, Song B, Rojaee R, Shokuhfar T, Pan YY, Lu J, Shahbazian-Yassar R. Elevated-temperature 3D printing of hybrid solid-state electrolyte for Li-Ion batteries. Adv Mater. 2018. https://doi.org/10.1002/adma.201800615.
19. Ye TT, Li LH, Zhang Y. Recent progress in solid electrolytes for energy storage devices. Adv Funct Mater. 2020;30:202000077.
20. Tian XC, Jin J, Yuan SQ, Chua CK, Tor SB, Zhou K. Emerging 3D-printed electrochemical energy storage devices: a critical review. Adv Energy Mater. 2017;7:1700127.
21. Cardoso RM, Kalinke C, Rocha RG, Dos Santos PL, Rocha DP, Oliveira PR, Janegitz BC, Bonacin JA, Richter EM, Munoz RA. Additive-manufactured (3D-printed) electrochemical sensors: a critical review. Anal Chim Acta. 2020;1118:73.
22. Chen CL, Li SP, Notten PHL, Zhang YH, Hao QL, Zhang XG, Lei W. 3D printed lithium-metal full batteries based on a high-performance three-dimensional anode current collector. ACS Appl Mater Interfaces. 2021;13:24785.

23. Kong DZ, Wang Y, Huang SZ, Zhang B, Lim YV, Sim GJ, YaP V, Ge Q, Yang HY. 3D printed compressible quasi-solid-state nickel-iron battery. ACS Nano. 2020;14:9675.
24. Cheng M, Deivanayagam R, Shahbazian-Yassar R. 3D Printing of electrochemical energy storage devices: a review of printing techniques and electrode/electrolyte architectures. Batter Supercaps. 2020;3:130.
25. Wang JW, Sun Q, Gao XJ, Wang CH, Li WH, Holness FB, Zheng M, Li RY, Price AD, Sun X, Sham TK, Sun XL. Toward high areal energy and power density electrode for Li-Ion batteries via optimized 3D printing approach. ACS Appl Mater Interfaces. 2018;10:39794.
26. Chung KC, Shu MH, Wang YC, Huang JC, Lau EM. 3D printing technologies applied to the manufacturing of aircraft components. Mod Phys Lett B. 2020;34:2040018.
27. Yan Q, Dong HH, Su J, Han JH, Song B, Wei QS, Shi YS. A review of 3D printing technology for medical applications. Eng PRC. 2018;4:729.
28. Park SH, Kaur M, Yun D, Kim WS. Hierarchically Designed electron paths in 3D printed energy storage devices. Langmuir. 2018;34:10897.
29. Qi Z, Ye JC, Chen W, Biener J, Duoss EB, Spadaccini CM, Worsley MA, Zhu C. 3D-printed, superelastic polypyrrole-graphene electrodes with ultrahigh areal capacitance for electrochemical energy storage. Adv Mater Technol. 2018;3:1800053.
30. Gao TT, Zhou Z, Yu JY, Zhao J, Wang GL, Cao DX, Ding B, Li YJ. 3D printing of tunable energy storage devices with both high areal and volumetric energy densities. Adv Energy Mater. 2019;9:1802578.
31. Oneil GD. Toward single-step production of functional electrochemical devices using 3D printing: progress, challenges, and opportunities. Curr Opin Electrochem. 2020;20:60.
32. Zhang F, Wei M, Viswanathan VV, Swart B, Shao YY, Wu G, Zhou C. 3D printing technologies for electrochemical energy storage. Nano Energy. 2017;40:418.
33. Yan K, Li J, Pan LJ, Shi Y. Inkjet printing for flexible and wearable electronics. APL Mater. 2020;8: 120705.
34. Sajedi-Moghaddam A, Rahmanian E, Naseri N. Inkjet-printing technology for supercapacitor application: current state and perspectives. ACS Appl Mater Interfaces. 2020;12:34487.
35. Wei M, Zhang F, Wang W, Alexandridis P, Zhou C, Wu G. 3D direct writing fabrication of electrodes for electrochemical storage devices. J Power Sources. 2017;354:134.
36. Kim H, Johnson J, Chavez LA, Garcia Rosales CA, Tseng T-LB, Lin Y. Enhanced dielectric properties of three phase dielectric MWCNTs/$BaTiO_3$/PVDF nanocomposites for energy storage using fused deposition modeling 3D printing. Ceram Int. 2018;44:9037.
37. Browne MP, Redondo E, Pumera M. 3D printing for electrochemical energy applications. Chem Rev. 2020;120:2783.
38. Nofal M, Pan Y, Al-Hallaj S. Selective laser sintering of phase change materials for thermal energy storage applications. Procedia Manuf. 2017;10:851.
39. Gao WL, Pumera M. 3D printed nanocarbon frameworks for Li-ion battery cathodes. Adv Funct Mater. 2021;31:2007285.
40. Foster CW, Down MP, Zhang Y, Ji X, Rowley-Neale SJ, Smith GC, Kelly PJ, Banks CE. 3D printed graphene based energy storage devices. Sci Rep. 2017;7:42233.
41. Ghosh K, Pumera M. MXene and MoS_{3-x} coated 3D-printed hybrid electrode for solid-state asymmetric supercapacitor. Small Methods. 2021. https://doi.org/10.1002/adma.202100451.
42. Chang P, Mei H, Zhou SX, Dassios KG, Cheng LF. 3D printed electrochemical energy storage devices. J Mater Chem A. 2019;7:4230.
43. Cha H, Lee Y, Kim J, Park M, Cho J. Flexible 3D interlocking lithium-ion batteries. Adv Energy Mater. 2018;8:1801917.
44. Zhang W, Liu HZ, Zhang XN, Li XJ, Zhang GH, Cao P. 3D printed micro-electrochemical energy storage devices: from design to integration. Adv Funct Mater. 2021;31:2104909.
45. Zhang QH, Zhou JQ, Chen ZH, Xu C, Tang W, Yang GZ, Lai CY, Xu QJ, Yang JH, Peng CX. Direct ink writing of moldable electrochemical energy storage devices: ongoing progress, challenges, and prospects. Adv Eng Mater. 2021;23:2100068.
46. Zhao JX, Zhang Y, Zhao XX, Wang RT, Xie JX, Yang CF, Wang JJ, Zhang QC, Li LL, Lu CH, Yao YG. Direct ink writing of adjustable electrochemical energy storage device with high gravimetric energy densities. Adv Funct Mater. 2019;29:1900809.
47. Yu LH, Li WP, Wei CH, Yang QF, Shao YL, Sun JY. 3D Printing of NiCoP/Ti_3C_2 MXene architectures for energy storage devices with high areal and volumetric energy density. Nanomicro Lett. 2020;12:143.
48. Li B, Hu NT, Su YJ, Yang Z, Shao F, Li G, Zhang CR, Zhang YF. Direct inkjet printing of aqueous inks to flexible all-solid-state graphene hybrid micro-supercapacitors. ACS Appl Mater Interfaces. 2019;11:46044.
49. Jiang YZ, Cheng M, Shahbazian-Yassar R, Pan Y. Direct ink writing of wearable thermoresponsive supercapacitors with rGO/CNT composite electrodes. Adv Mater Technol. 2019;4:1900691.
50. Yang PH, Fan HJ. Inkjet and extrusion printing for electrochemical energy storage: a minireview. Adv Mater Technol. 2020;5:2000217.
51. Zhang CJ, Mckeon L, Kremer MP, Park SH, Ronan O, Seral-Ascaso A, Barwich S, Coileain CO, Mcevoy N, Nerl HC, Anasori B, Coleman JN, Gogotsi Y, Nicolosi V. Additive-free MXene inks and direct printing of micro-supercapacitors. Nat Commun. 2019;10:1795.
52. Chen C, Jiang JM, He WJ, Lei W, Hao QL, Zhang XG. 3D printed high-loading lithium-sulfur battery toward wearable energy storage. Adv Funct Mater. 2020;30:1909469.
53. Pang YK, Cao YT, Chu YH, Liu MH, Snyder K, Mackenzie D, Cao CY. Additive manufacturing of batteries. Adv Funct Mater. 2019;30:1906244.
54. Huang JG, Qin Q, Wang J. A review of stereolithography: processes and systems. Processes. 2020;8:1138.
55. Kanai T, Tsuchiya M. Microfluidic devices fabricated using stereolithography for preparation of monodisperse double emulsions. Chem Eng J. 2016;290:400.
56. Bartolomeua F, Buciumeanub M, Pintoc E, et al. 316L stainless steel mechanical and tribological behavior—A comparison between selective laser melting, hot pressing and conventional casting. Addit. Manuf. 2017;16:81–89.
57. Nagarajan B, Hu ZH, Song X, Zhai W, Wei J. Development of micro selective laser melting: the state of the art and future perspectives. Eng PRC. 2019;5:702.
58. Ambrosi A, Moo JGS, Pumera M. Helical 3D-printed metal electrodes as custom-shaped 3D platform for electrochemical devices. Adv Funct Mater. 2016;26:698.
59. Zhao JX, Lu HY, Zhao XX, Malyi OI, Peng JH, Lu CH, Li XF, Zhang YY, Zeng ZY, Xing GC, Tang YX. Printable ink design towards customizable miniaturized energy storage devices. ACS Mater Lett. 2020;2:1041.
60. Wang YL, Wang GL, Cao CY, Zhang Y, Tang C, Liu HG, Shen JF, Li L. 3D printable ink for double-electrical-layer-enhanced electrode of microsupercapaitors. J Power Sources. 2021;512:230468.
61. Park S, Nenov NS, Ramachandran A, Chung K, Hoon Lee S, Yoo J, Yeo J-G, Bae C-J. Development of highly energy densified ink for 3D printable batteries. Energy Technol. 2018;6:2058.
62. Moser S, Kenel C, Wehner LA, Spolenak R, Dunand DC. 3D ink-printed, sintered porous silicon scaffolds for battery applications. J Power Sources. 2021;507:230298.

63. Zhang YZ, Wang Y, Jiang Q, El-Demellawi JK, Kim H, Alshareef HN. MXene printing and patterned coating for device applications. Adv Mater. 2020. https://doi.org/10.1002/adma.201908486.
64. Glasser A, Cloutet E, Hadziioannou G, Kellay H. Tuning the rheology of conducting polymer inks for various deposition processes. Chem Mater. 2019. https://doi.org/10.1021/acs.chemmater.9b01387.
65. Jiang YQ, Xu Z, Huang TQ, Liu YJ, Guo F, Xi JB, Gao WW, Gao C. Direct 3D printing of ultralight graphene oxide aerogel microlattices. Adv Funct Mater. 2018;28:1707024.
66. Akuzum B, Maleski K, Anasori B, Lelyukh P, Alvarez NJ, Kumbur EC, Gogotsi Y. Rheological characteristics of 2D titanium carbide (MXene) dispersions: a guide for processing MXenes. ACS Nano. 2018;12:2685.
67. Yang WJ, Yang J, Byun JJ, Moissinac FP, Xu J, Haigh SJ, Domingos M, Bissett MA, Dryfe RAW, Barg S. 3D printing of freestanding MXene architectures for current-collector-free supercapacitors. Adv Mater. 2019. https://doi.org/10.1002/adma.201902725.
68. Lin LY, Ning HM, Song SF, Xu CH, Hu N. Flexible electrochemical energy storage: the role of composite materials. Compos Sci Technol. 2020;192:108102.
69. Xu ZC, Zhang FQ, Zhang MY, Wang P. Energy storage development trends and key issues for future energy system modeling. IOP Conf Ser: Earth Environ Sci. 2020;526:0121141.
70. Rincón RA, Heydenrych G. Batteries and supercaps: the future of electrochemical energy storage. Batter Supercaps. 2018;1:3.
71. Wang CG, Zhao SS, Song XX, Wang NN, Peng HL, Su J, Zeng SY, Xu XJ, Yang J. Suppressed dissolution and enhanced desolvation in core-shell MoO_3@TiO_2 nanorods as a high-rate and long-life anode material for proton batteries. Adv Energy Mater. 2022;12:2200157.
72. Ma HY, Chen HW, Hu YJ, Yang BJ, Feng JZ, Xu YT, Sun YL, Cheng HH, Li C, Yan XB, Qu LT. Aqueous rocking-chair aluminum-ion capacitors enabled by a self-adaptive electrochemical pore-structure remolding approach. Energy Environ. 2022;15:1131.
73. Kang WB, Zeng L, Ling SW, Zhang CH. 3D printed supercapacitors toward trinity excellence in kinetics, energy density, and flexibility. Adv Energy Mater. 2021;11:2100020.
74. Tagliaferri S, Nagaraju G, Panagiotopoulos A, Och M, Cheng G, Iacoviello F, Mattevi C. Aqueous inks of pristine graphene for 3D printed microsupercapacitors with high capacitance. ACS Nano. 2021;15:15342.
75. Zhu C, Liu TY, Qian F, Chen W, Chandrasekaran S, Yao B, Song Y, Duoss EB, Kuntz JD, Spadaccini CM, Worsley MA, Li Y. 3D printed functional nanomaterials for electrochemical energy storage. Nano Today. 2017;15:107.
76. Lee HC, Liu WW, Chai SP, Mohamed AR, Aziz A, Khe C-S, Hidayah NMS, Hashim U. Review of the synthesis, transfer, characterization and growth mechanisms of single and multilayer graphene. RSC Adv. 2017;7:15644.
77. Yao B, Chandrasekaran S, Zhang H, Ma A, Kang J, Zhang L, Lu X, Qian F, Zhu C, Duoss EB, Spadaccini CM, Worsley MA, Li Y. 3D-printed structure boosts the kinetics and intrinsic capacitance of pseudocapacitive graphene aerogels. Adv Mater. 2020. https://doi.org/10.1002/adma.201906652.
78. Lacey SD, Kirsch DJ, Li Y, Morgenstern JT, Zarket BC, Yao YG, Dai J, Garcia LQ, Liu BY, Gao TT, Xu SM, Raghavan SR, Connell JW, Lin Y, Hu LB. Extrusion-based 3D printing of hierarchically porous advanced battery electrodes. Adv Mater. 2018. https://doi.org/10.1002/adma.201705651.
79. Gu YF, Zhang Y, Shi YH, Zhang LF, Xu XH. 3D all printing of polypyrrole nanotubes for high mass loading flexible supercapacitor. ChemistrySelect. 2019;4:10902.
80. Areir M, Xu Y, Harrison D, Fyson J. 3D printing of highly flexible supercapacitor designed for wearable energy storage. Mater Sci Eng B. 2017;226:29.
81. Aeby X, Poulin A, Siqueira G, Hausmann MK, Nystrom G. Fully 3D printed and disposable paper supercapacitors. Adv Mater. 2021. https://doi.org/10.1002/adma.202101328.
82. Wang YY, Wang ZJ, Yu XL, Li BH, Kang FY, He YB. Hierarchically structured carbon nanomaterials for electrochemical energy storage applications. J Mater Res. 2018;33:1058.
83. Ni JF, Li Y. Carbon nanomaterials in different dimensions for electrochemical energy storage. Adv Energy Mater. 2016;6:1600278.
84. Roman J, Neri W, Fierro V, Celzard A, Bentaleb A, Ly I, Zhong J, Derre A, Poulin P. Lignin-graphene oxide inks for 3D printing of graphitic materials with tunable density. Nano Today. 2020;33:100881.
85. Tang XW, Zhou H, Cai ZC, Cheng DD, He PS, Xie PW, Zhang D, Fan TX. Generalized 3D printing of graphene-based mixed-dimensional hybrid aerogels. ACS Nano. 2018;12:3502.
86. Yao B, Chandrasekaran S, Zhang J, Xiao W, Qian F, Zhu C, Duoss EB, Spadaccini CM, Worsley MA, Li Y. Efficient 3D printed pseudocapacitive electrodes with ultrahigh MnO_2 loading. Joule. 2019;3:459.
87. Shen K, Ding JW, Yang SB. 3D printing quasi-solid-state asymmetric micro-supercapacitors with ultrahigh areal energy density. Adv Energy Mater. 2018;8:1800408.
88. Balducci A. Ionic liquids in lithium-ion batteries. Top Curr Chem (Cham). 2017;375:20.
89. Tang YW, Lee JM, Fu GT. ChemElectroChem: beyond lithium-ion batteries. ChemElectroChem. 2021;8:1149.
90. Jin S, Jiang Y, Ji HX, Yu Y. Advanced 3D current collectors for lithium-based batteries. Adv Mater. 2018. https://doi.org/10.1002/adma.201802014.
91. Sun K, Wei TS, Ahn BY, Seo JY, Dillon SJ, Lewis JA. 3D printing of interdigitated Li-ion microbattery architectures. Adv Mater. 2013;25:4539.
92. Fu K, Wang Y, Yan C, Yao Y, Chen Y, Dai J, Lacey S, Wang Y, Wan J, Li T, Wang Z, Xu Y, Hu L. Graphene oxide-based electrode inks for 3D-printed lithium-ion batteries. Adv Mater. 2016;28:2587.
93. Shen K, Mei HL, Li B, Ding JW, Yang SB. 3D printing sulfur copolymer-graphene architectures for Li-S batteries. Adv Energy Mater. 2017;8:1701527.
94. Fan ZD, Wei CH, Yu LH, Xia Z, Cai JS, Tian ZN, Zou GF, Dou SX, Sun JY. 3D printing of porous nitrogen-doped Ti_3C_2 MXene scaffolds for high-performance sodium-ion hybrid capacitors. ACS Nano. 2020;14:867.
95. Zhang TY, Ran F. Design strategies of 3D carbon-based electrodes for charge/ion transport in lithium ion battery and sodium ion battery. Adv Funct Mater. 2021;31:2010041.
96. Zhu S, Wang CD, Shou HW, Zhang PJ, Wan P, Guo X, Yu Z, Wang WJ, Chen SM, Chu WS, Song L. In situ architecting endogenous heterojunction of MoS_2 coupling with Mo_2 CTx MXenes for optimized Li(+) storage. Adv Mater. 2022. https://doi.org/10.1002/adma.202108809.
97. Lu CX, Li AR, Li GZ, Yan Y, Zhang MY, Yang QL, Zhou W, Guo L. S-Decorated porous Ti_3 C_2 MXene combined with in situ forming Cu_2Se as effective shuttling interrupter in Na-Se batteries. Adv Mater. 2021. https://doi.org/10.1002/adma.202008414.
98. Kayali E, Vahidmohammadi A, Orangi J, Beidaghi M. Controlling the dimensions of 2D MXenes for ultrahigh-rate pseudocapacitive energy storage. ACS Appl Mater Interfaces. 2018;10:25949.
99. Li XR, Li HP, Fan XQ, Shi XL, Liang JJ. 3D-printed stretchable micro-supercapacitor with remarkable areal performance. Adv Energy Mater. 2020;10:1903794.

100. Yu LH, Fan ZD, Shao YL, Tian ZN, Sun JY, Liu ZF. Versatile N-doped MXene ink for printed electrochemical energy storage application. Adv Energy Mater. 2019;9:1901839.
101. Zheng SH, Wang H, Das P, Zhang Y, Cao YX, Ma JX, Liu SF, Wu ZS. Multitasking MXene inks enable high-performance printable microelectrochemical energy storage devices for all-flexible self-powered integrated systems. Adv Mater. 2021. https://doi.org/10.1002/adma.202005449.
102. Zhang CJ, Park SH, Seral-Ascaso A, Barwich S, Mcevoy N, Boland CS, Coleman JN, Gogotsi Y, Nicolosi V. High capacity silicon anodes enabled by MXene viscous aqueous ink. Nat Commun. 2019;10:849.
103. Deng YQ, Shang TX, Wu ZT, Tao Y, Luo C, Liang JC, Han DL, Lyu R, Qi CS, Lv W, Kang FY, Yang QH. Fast gelation of Ti_3C_2Tx MXene initiated by metal ions. Adv Mater. 2019. https://doi.org/10.1002/adma.201902432.
104. Wang Q, Zhou YH, Zhao X, Chen K, Bingni G, Yang T, Zhang HT, Yang WQ, Chen J. Tailoring carbon nanomaterials via a molecular scissor. Nano Today. 2021;36:101033.
105. Wang Q, Liu FY, Jin ZY, Qiao XR, Huang HC, Chu X, Xiong D, Zhang HT, Liu Y, Yang WQ. Hierarchically divacancy defect building dual-activated porous carbon fibers for high-performance energy-storage devices. Adv Funct Mater. 2020;30:2002580.
106. Wang Q, Chen YY, Jiang X, Qiao XR, Wang YH, Zhao HB, Pu B, Yang WQ. Self-assembly defect-regulating superstructured carbon. Energy Stor Mater. 2022;48:164.
107. Down MP, Martínez-Periñán E, Foster CW, Lorenzo E, Smith GC, Banks CE. Next-generation additive manufacturing of complete standalone sodium-ion energy storage architectures. Adv Energy Mater. 2019;9:1803019.
108. Wang D, Han CP, Mo F, Yang Q, Zhao YW, Li Q, Liang GJ, Dong BB, Zhi C. Energy density issues of flexible energy storage devices. Energy Stor Mater. 2020;28:264.
109. Orangi J, Hamade F, Davis VA, Beidaghi M. 3D printing of additive-free 2D Ti_3C_2Tx (MXene) ink for fabrication of micro-supercapacitors with ultra-high energy densities. ACS Nano. 2020;14:640.
110. Jagadale AD, Rohit RC, Shinde SK, Kim DY. Materials development in hybrid zinc-ion capacitors. ChemNanoMat. 2021;7:1082.
111. Fan ZD, Jin J, Li C, Cai JS, Wei CH, Shao YL, Zou GF, Sun JY. 3D-printed Zn-Ion hybrid capacitor enabled by universal divalent cation-gelated additive-free Ti_3C_2 MXene ink. ACS Nano. 2021;15:3098.